CHAPTER 8

YAGI-UDA, SPIRAL AND LOG PERIODIC ANTENNAS

8.1 YAGI-UDA ANTENNAS

In Chapter 3 it is shown that array antennas can be used to increase directivity. In the arrays all elements were active, requiring a direct connection to each element by a feed network. Array feed networks are considerably simplified if only a few elements are fed directly. Such an array is referred to as a parasitic array. The elements that are not directly driven (called parasites) receive their excitation by near-field coupling from the driven elements. A parasitic linear array of parallel dipoles is called a Yagi-Uda antenna, a Yagi-Uda array, or simply "Yagi." Yagi-Uda antennas are very popular because of their simplicity and relatively medium gain.

To understand the principles of operation for a three element Yagi, a driven element (or "driver") is considered first and add parasites to the array. A driven element is considered that is a resonant half-wave dipole. If a parasitic element is positioned very close to it, it is excited by the driven element with roughly equal amplitudes, so the field incident on the parasite is

$$E_{incident} = E_{\text{driver}} \tag{8.1}$$

A current is excited on the parasite and the resulting radiated electric field, also tangent to the wire, is equal to in amplitude and opposite in phase to the incident wave. This is because the electric field arriving at the parasite from the driver is tangential to it and the total electric field tangential to a good conductor is zero. Thus, the field radiated by the parasite is such that the total tangential field on the parasite is zero, or $0 = E_{\text{incident}} + E_{\text{parasite}}$. Combining this fact with (8.1) gives

$$E_{\text{parasite}} = -E_{\text{incident}} = -E_{\text{driver}} \tag{8.2}$$

From array theory, it is known that two closely spaced, equal amplitude, opposite phase elements will have an endfire pattern. The pattern of this simple two-element parasitic array for 0.04λ spacing is shown in Figure 8.1.

The simplistic beauty of the Yagi is revealed by lengthening the parasite. The dual endfire beam is changed to a more desirable single endfire beam. This effect is illustrated for the two-element parasite array of Figure 8.2. The driver is a dipole of length 0.4781λ, which is a half-wave resonant length when operated in free space. The parasite is a straight wire of length 0.49λ and spaced a distance 0.04λ away from the driver. The H-plane pattern in Figure 8.2b obtained from the numerical methods demonstrates the

general trend of a parasite that is longer than the driver: a single main beam occurs in the endfire direction from the parasite to the driver along the line of array. Such a parasite is called a *reflector* because it appears to reflect radiation from the driver.

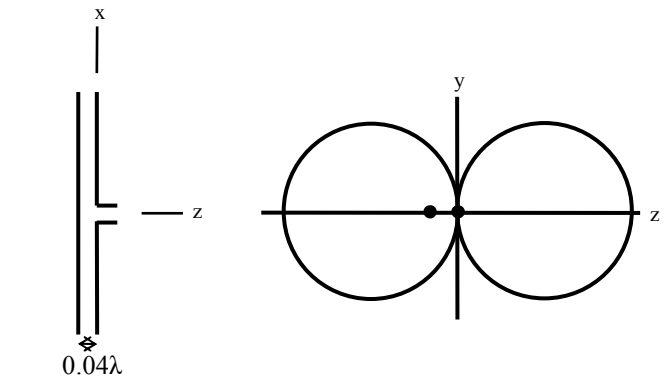

(a) Array configuration

(b) H-plane pattern computed from simple array theory.

Figure 8.1 A two-element arrays of half-wave resonant dipoles, one a driver and the other a parasite. The currents on both are equal in amplitude and opposite in phase.

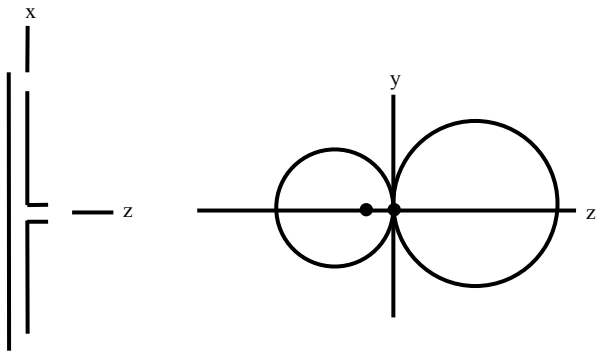

(a) Array configuration

(b) H-plane pattern computed from numerical methods.

Figure 8.2 Two-element Yagi-Uda antenna consisting of a driver of length 0.4781λ and a reflector of length 0.49λ spaced 0.04λ away. The wire radius for both is 0.001λ.

If the parasite is shorter than the driver, but now placed on the other side of the driver, the pattern effect is similar to that when using a reflector in the sense that main beam enhancement is in the same direction. The parasite is then referred to as a *director* since it appears to direct radiation in the direction from the driver toward the director. The parasitic array in Figure 8.3a consisting of a driver and a director has the pattern shown in Figure 8.3b.

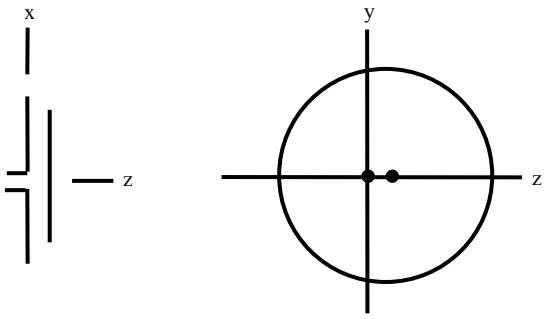

(a) Array configuration

(b) H-plane pattern computed from numerical methods.

Figure 8.3 Two-element Yagi-Uda antenna consisting of a driver of length 0.4781λ and a director of length 0.45λ spaced 0.04λ away. The wire radius for both is 0.001λ.

The single endfire beam created by the use of a reflector or a director alone with a driver suggests that even further enhancement could be achieved with a reflector and a director on opposite sides of a driver. An example of a three-element Yagi is shown in Figure 8.4a, which is a combination of the geometries of Figs. 8.2a and 8.3a. The pattern of Figure 8.4b is improved over that of either two-element array. The *E*-plane pattern for the three-element Yagi is shown in Figure 8.4c. It is essentially equal to the H-plane pattern multiplied by the element factor of the array, which is that of a half-wave dipole. Again, these patterns were obtained by numerical solution for exceptionally small element spacing (0.04λ).

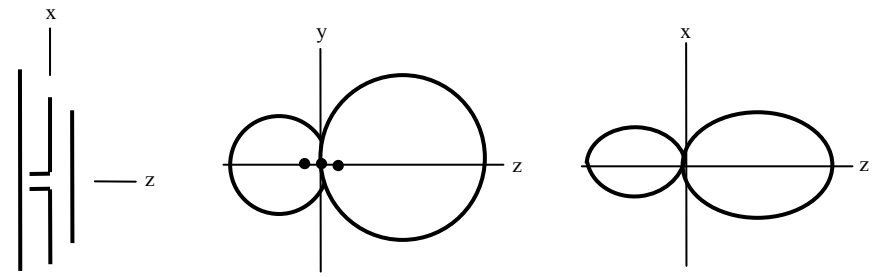

(a) Array configuration.

(b) H-plane pattern computed from numerical methods.

(c) E-plane pattern computed from numerical methods.

Figure 8.4 Three-element Yagi-Uda antennas consisting of a driver of length 0.4781λ, a reflector of 0.49λ, and a director of length 0.45λ, each spaced only 0.04λ apart. The wire radius for each is 0.001λ.

The general Yagi configuration is shown in Figure 8.5. The maximum directivity obtainable from a three-element Yagi is about 9 dBi or 7 dBd. The optimum reflector spacing S_R (for maximum directivity) is between 0.15 and 0.25λ.

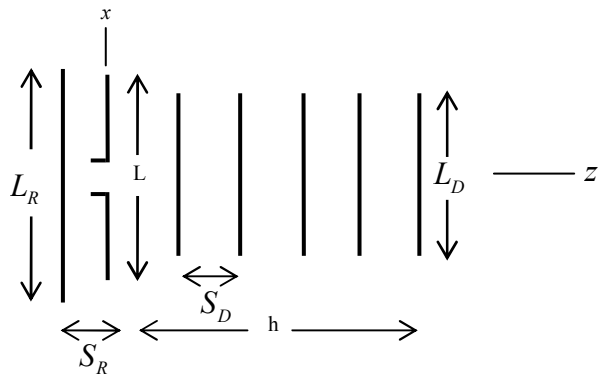

Figure 8.5 General Yagi-Uda antenna.

Director-to-director spacings are typically 0.2 to 0.35 wavelengths, with the larger spacings being more common for long arrays and closer spacings for shorter arrays. Typically, the reflector length is 0.5λ and the driver is of resonant length when no parasitic elements are present the director lengths are typically 10 to 20% shorter than their resonant length, the exact length being rather sensitive to the number of directors N_D and the inter-director spacing S_D.

The increase in gain of the Yagi is smaller as more directors are added to the array (if we assume S_D is fixed) since the Yagi is not uniformly excited. In fact, the addition of the directors up to about 5 or 6 provides a significant increase in gain expressed in dB, whereas the addition of more directors is beyond the "point of diminishing returns" as Figure 8.6 shows. Figure 8.6 plots the gain versus of number of elements *N* in the array (including one reflector and one driver) for an inter-element spacing for all elements of $S_R = S_D = 0.15\lambda$. It should be noted that adding one director to increase *N* from 3 to 4 gives about a 1-dB gain increase, whereas adding one director to increase *N* from 9 to 10 yielded only about an additional 0.2-dB gain.

The addition of more reflector elements results in a fractional dB increase in gain and is usually not done. The main effects of the reflector are on the driving points impedance at the feed point and on the back lobe of the array. Pattern shape, and therefore gain, are mostly controlled by the director elements. The director spacing and director length are interrelated, but the more sensitive parameter is the director length, which becomes more critical as the boom length increases.

Boom lengths from 0.2 to 4.2λ are used. if a metal boom is used. A metal boom may be used because the voltage distribution on the parasitic elements goes through a zero at the

element center. Ideally, an infinitely thin metallic boom down the center of the array would not change the voltage distribution. However, metallic booms of practical size to have an effect that must be compensated for by increasing the parasitic element lengths as shown in Figure 8.7. Alternatively, the parasitic elements may be insulated from the boom, in which case no compensation is required.

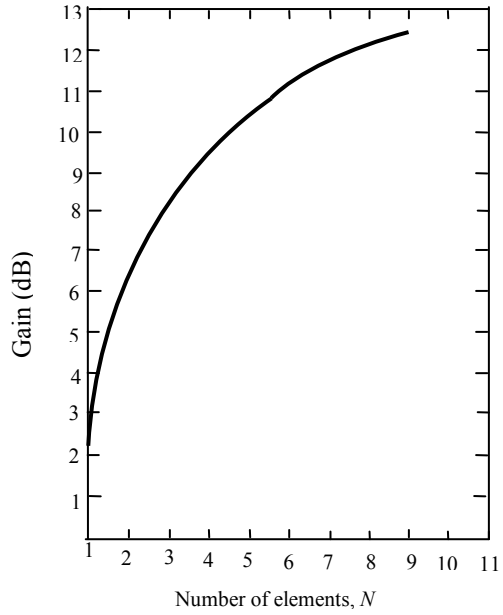

Figure 8.6 Gain of a typical Yagi-Uda antenna versus the total number of elements. The element spacings $S_R = S_D = 0.15\lambda$. The conductor diameters are 0.0025λ.

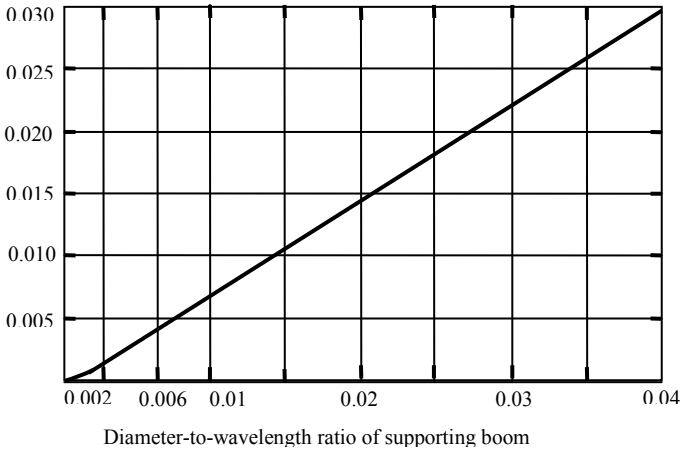

Figure 8.7 Graph showing effect of supporting metal boom on the length of Yagi parasitic elements.

The Yagi is one of the more popular antennas used in the HF-VHF-UHF frequency range. It provides moderately high gain while offering low weight and low cost. It has a relatively narrow bandwidth (e.g., a few percent), which may be improved somewhat by using feeds other than a dipole, such as a folded dipole. The folded dipole also provides a higher input impedance than a dipole even though the driving point impedance of both are usually reduced considerably from their self-impedances by mutual coupling effects. Further, increased gain can be obtained by arraying or 'stacking" Yagi antennas. Maximum gain results for a separation of almost one wavelength. Thus, for a given application, if a somewhat narrow bandwidth can be tolerated, the Yagi-Uda antenna can provide good gain at low cost.

8.2 THE FREQUENCY-INDEPENDENT CONCEPT: RUMSEY'S PRINCIPLE.

Victor H. Rumsey developed and introduced a new way of looking at the antennas and their operation as a function of the frequency. Rumsey was intrigued with Mushiake's observation that *self-complementary antennas* have a constant impedance of $Z_0/2$, or half the intrinsic impedance of space, at all frequencies. This is remarkable since there is an infinity of self-complementary shapes. A self-complementary planar antenna has a metal area congruent to the open area, i.e., the two areas can be brought into coincidence by a rigid motion. The metal and open areas are congruent since a rotation of either brings both into coincidence. The slot and complementary dipole antennas of Chapter 2 are similarly related but usually require a translation for coincidence. Mushiake's $Z_0/2$ result comes directly from booker's relation for complementary slots and dipoles.

Rumsey's principle is that the impedance and pattern properties of an antenna will be frequency independent if the antenna shape is specified only in terms of angles. Thus, an infinite logarithmic spiral should meet the requirement.The biconical antenna is an example of an antenna that can be specified only in terms of the included cone angle, but it is frequency independent only if it is infinitely long. When truncated (without a matched termination) there is a reflected wave from the ends of the cones which results in modified impedance and pattern characteristics.

To meet the frequency-independent requirement in a finite structure requires that the current attenuate along the structure and be negligible at the point of truncation. For radiation and attenuation to occur charge must be accelerated (or decelerated) and this happens when a conductor is curved or bent normally to the direction in which the charge is traveling. Thus the curvature of a spiral results in radiation and attenuation so that, even when truncated, the spiral provides frequency-independent operation over a wide bandwidth. Rumsey's principle was implemented experimentally by John. D. Dyson at the university of Illinois, who constructed the first practical frequency-independent spiral antennas in 1958, first the bidirectional planar spiral and then the unidirectional conical spiral. These two types are described in the next two sections.

8.2.1 The Frequency-Independent Planar Log-Spiral Antenna

The equation for a *logarithmic (or log) spiral* is given by

$$r = a^{\theta} \tag{8.3}$$

or
$$\ln r = \theta \ln a \tag{8.4}$$

where, referring to Figure 8.8,

r = radial distance to point P on spiral
θ = angle with respect to x axis
a = a constant

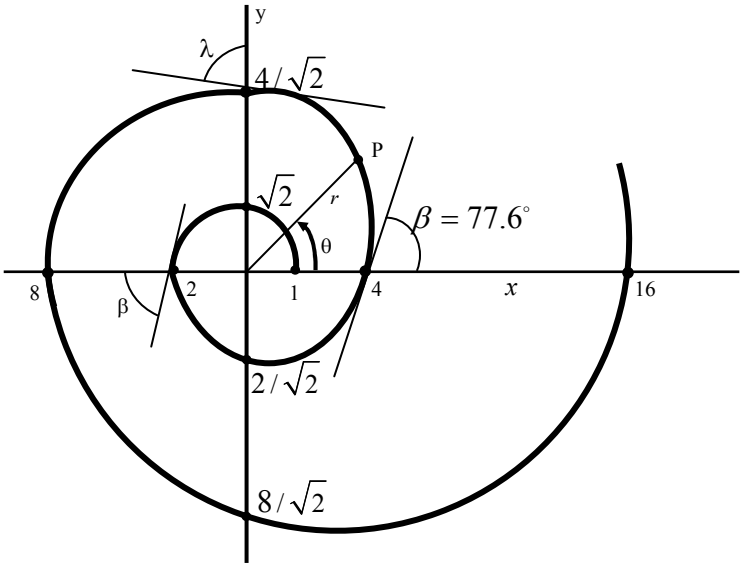

Figure 8.8 Logarithmic or log spiral.

From (8.3), the rate of change of radius with angle is

$$\frac{\mathrm{d}r}{\mathrm{d}\theta} = a^{\theta} \ln a = r \ln a \tag{8.5}$$

The constant a in (8.5) is related to the angle β between the spiral and a radial line from the origin as given by

$$\ln a = \frac{dr}{r\,d\theta} = \frac{1}{\tan\beta} \tag{8.6}$$

Thus, from (8.6) and (8.4),

$$\theta = \tan\beta \ln r \tag{8.7}$$

The log spiral in Figure 8.9 was constructed so as to make r =1 at θ = 0 and r = 2 at θ = π. These conditions determine the value of the constants a and β. Thus, from (8.6) and (8.7), $\beta = 77.6^\circ$, and a = 1.247. Thus, the shape of the spiral is determined by the anglel β which is the same for all points on the spiral.

Let a second log spiral, identical in form to the one in Figure 8.9, be generated by an angular rotation δ so that (8.3) becomes

$$r_2 = a^{\theta-\delta} \tag{8.8}$$

and a third and fourth spiral given by

$$r_3 = a^{\theta-\pi} \tag{8.9}$$

and

$$r_4 = a^{\theta-\pi-\delta} \tag{8.10}$$

Then, for a rotation $\delta = \pi/2$ we have 4 spirals at 90° angles. Metalizing the areas between spirals 1 and 4 and 2 and 3, with the other areas open, self-complementary and congruence conditions are satisfied. Connecting a generator or receiver across the inner terminals, we obtain Dyson's frequency-independent planar spiral antenna of Figure 8.9.

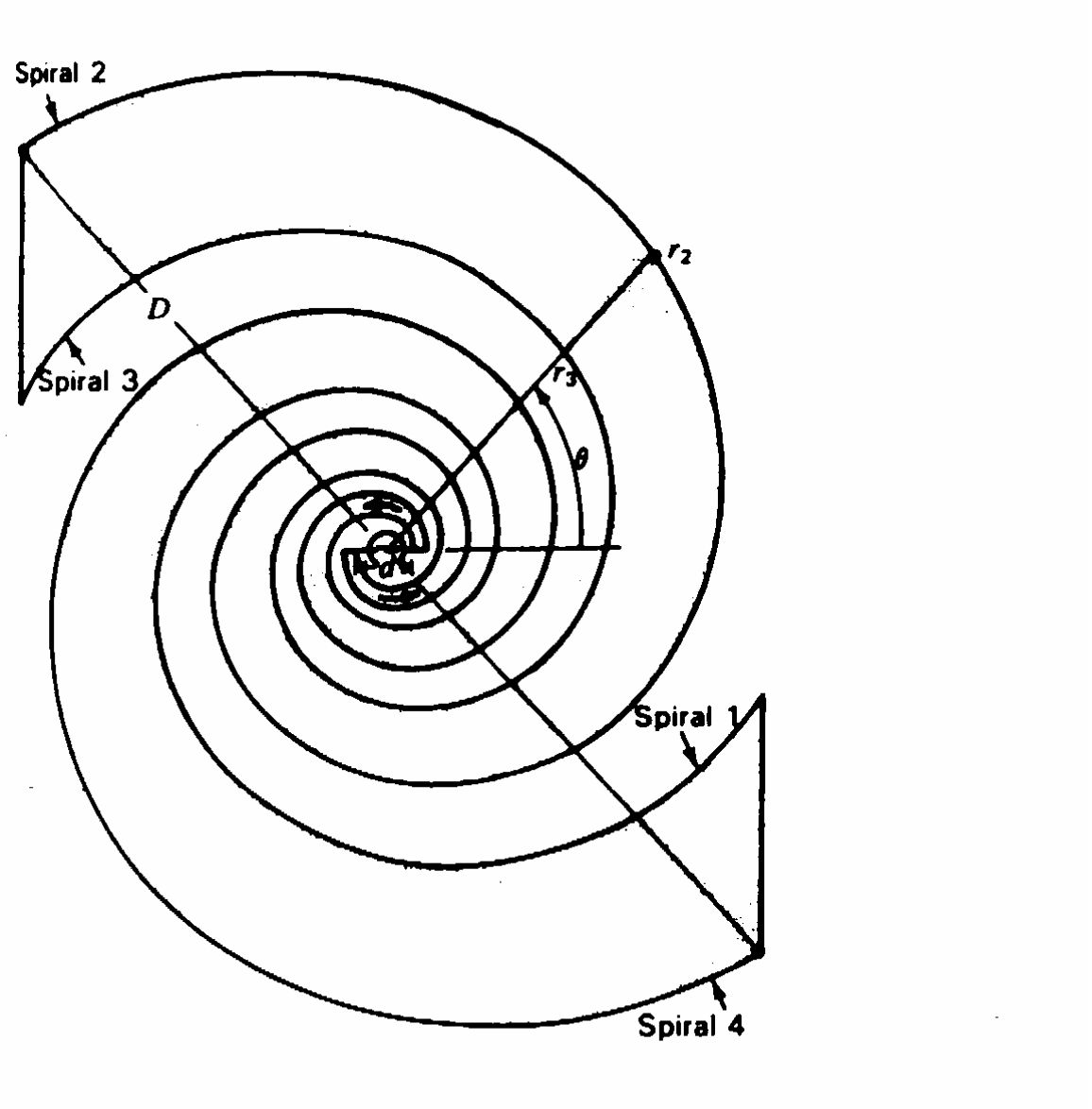

Figure 8.9 Frequency-independent planar spiral antenna.

The arrows indicate the direction of outgoing waves traveling along the conductors resulting in right-circularly polarized (RHCP) radiation outward from the page and left-circularly polarized (LHCP) radiation into the page. The high-frequency limit of operation is determined by the spacing d of the input terminal and the low-frequency limit by the overall diameter D. The ratio D/d for the antenna of Figure 8.9 is about 25 to 1. If we take $d = \lambda/10$ at the high-frequency limit and $D = \lambda/2$ at the low-frequency limit, the antenna bandwidth is 5 to 1. The spiral should be continued to a smaller radius but, for clarity, the termination separation shown in Figure 8.10 is larger than it should be. Halving it doubles the bandwidth.

In practice it is more convenient to cut the slots for the antenna from a large ground plane, as done by Dyson, and feed the antenna with a coaxial cable bonded to one of the spiral arms as in Figure 8.10, the spiral acting as a balun. A dummy cable may be bonded to the other arm for symmetry but is not shown.

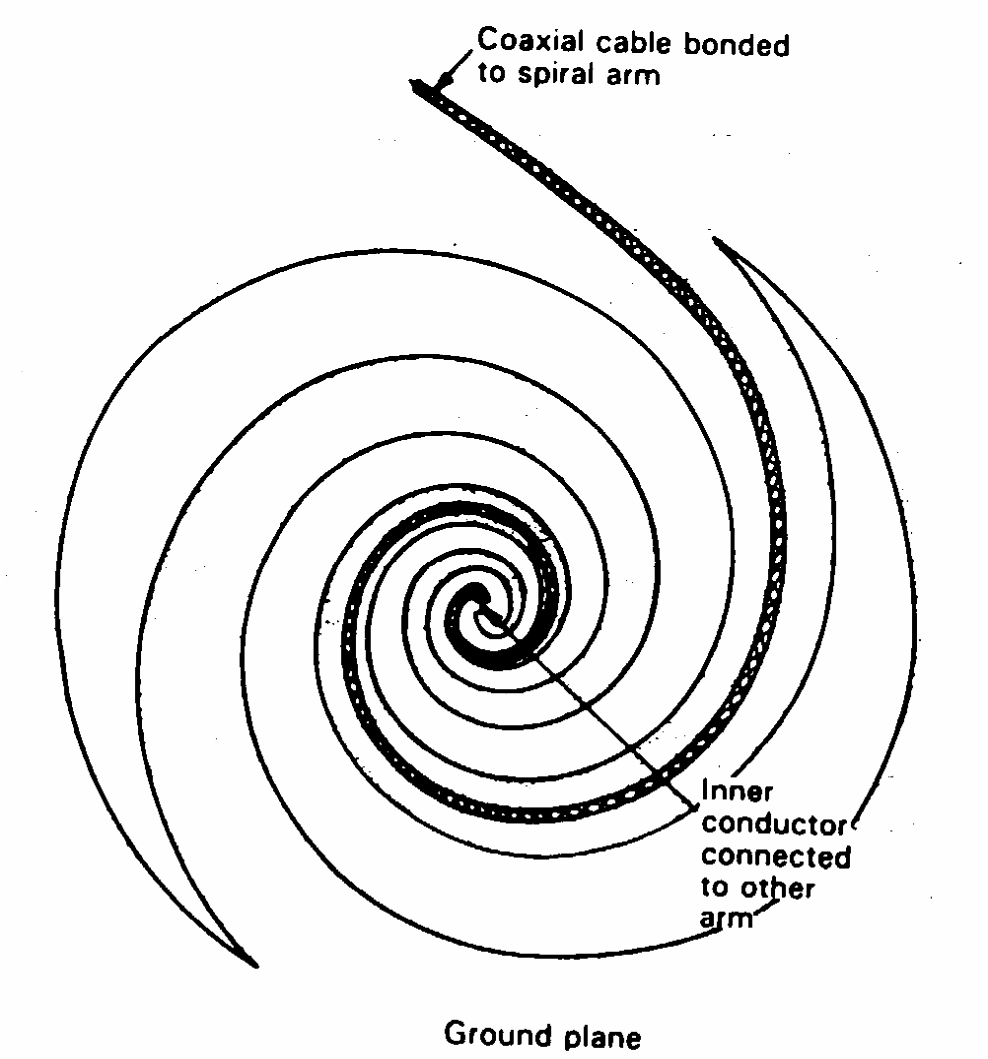

Figure 8.10 Frequency-independent planar spiral antenna cut from large ground plane.

Radiation for the antennas of Figs. 8.9 and 8.10 is bidirectional broadside to the plane of the spiral. The patterns in both directions have a single broad lobe so that the gain is only a few dBi. The input impedance depends on the parameters δ and a and the terminal separation. According to Dyson, typical values are in the range 50 to 100Ω , or considerably less than the theoretical $188\Omega\left(=Z_0/2\right)$. The smaller measured values are due to the finite thickness of spirals.

Referring to Figure 8.9, the ratio K of the radii across any arm, such as between spirals 2 and 3, is given by the ratio of (8.9) to (8.8), or

$$K = \frac{r_3}{r_2} = a^{-\pi+\delta} \tag{8.11}$$

For the antenna of Figure 8.10, $\delta = \pi/2$ so

$$K = \frac{r_3}{r_2} = a^{-\pi/2} = 0.707(=1/\sqrt{2}) \tag{8.12}$$

This is seen to be the ratio of the radial distances to the spiral of Figure 8.10 at successive 90° intervals.

8.3 LOG PERIODIC ANTENNA

A log-periodic antenna is another form of frequency-independent antenna and has a structural geometry such that its impedance and radiation characteristics repeat periodically as the logarithm of frequency. In practice, the variations over the frequency band of operation are minor.

The final phase in this metamorphosis of log-periodic antennas is the use of only parallel wire segments. This is the log-periodic dipole array of Figure 8.11. The log-periodic dipole array (LPDA) is a series-fed array of parallel wire dipoles of successively increasing lengths outward from the feed point at the apex. Note that the interconnecting feed lines cross over between adjacent elements.

A particularly successful method of constructing an LPDA is shown in Figure 8.12. A coaxial transmission line is run through the inside of one of the feed conductors. The outer conductor of the coax is attached to that conductor and the inner conductor of the coax is connected to the other conductor of the LPDA transmission line.

As shown in Figure 8.11, a wedge of enclosed angle α bounds the dipole lengths. The scale factor τ for the LPDA is

$$\tau = \frac{R_{n+1}}{R_n} < 1 \tag{8.13}$$

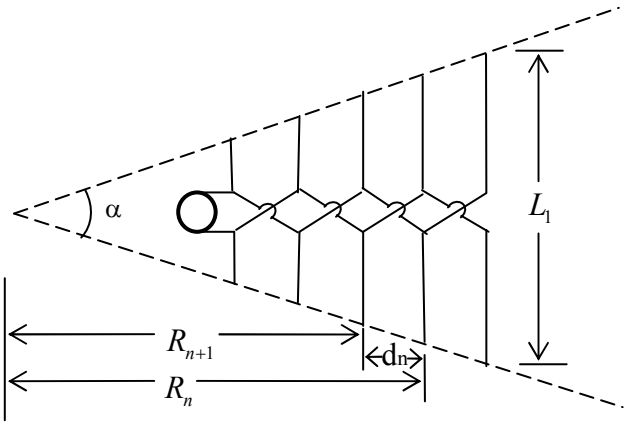

Figure 8.11 Log-periodic dipole array geometry.

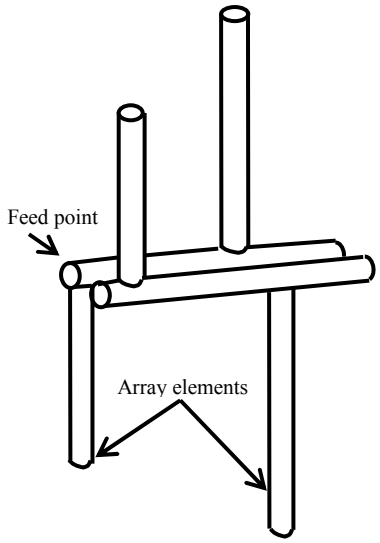

Figure 8.12 Construction details of the log-periodic dipole array.

Right triangles of enclosed angle $\alpha/2$ reveal that

$$\tan\frac{\alpha}{2} = \frac{L_n/2}{R_n} = \frac{L_{n+1}/2}{R_{n+1}} \tag{8.14}$$

Thus,

$$\frac{L_1}{R_1} = ... = \frac{L_n}{R_n} = \frac{L_{n+1}}{R_{n+1}} = ... = \frac{L_N}{R_N} \tag{8.15}$$

Using this result in (8.13) gives

$$\tau = \frac{R_{n+1}}{R_n} = \frac{L_{n+1}}{L_n} \tag{8.16}$$

The spacing factor for the LPDA is defined as

$$\sigma = \frac{d_n}{2L_n} \tag{8.17}$$

Where the element spacings as shown in Figure 8.12 are given by

$$d_n = R_n - R_{n+1} \tag{8.18}$$

But

$$R_{n+1} = \tau R_n \text{, so}$$

$$d_n = R_n - \tau R_n = (1-\tau)R_n \tag{8.19}$$

From (8.14), $R_n = L_n / 2\tan(\alpha/2)$. Using this in (8.19) yields

$$d_n = (1-\tau)\frac{L_n}{2\tan(\alpha/2)} \tag{8.20}$$

Substituting this in (8.17) gives

$$\sigma = \frac{d_n}{2L_n} = \frac{1-\tau}{4\tan(\alpha/2)} \tag{8.21}$$

or

$$\alpha = 2\tan^{-1}\left(\frac{1-\tau}{4\sigma}\right) \tag{8.22}$$

Combining (8.22) with (8.16), we note that all dimensions are scaled by

$$\tau = \frac{R_{n+1}}{R_n} = \frac{L_{n+1}}{L_n} = \frac{d_{n+1}}{d_n} \tag{8.23}$$

There is an active region for the LPDA, where the few dipoles near the one that is a half-wavelength long support much more current than do the other radiating elements. It is convenient to view the LPDA operation as being similar to that of a Yagi-Uda antenna. The longer dipole behind the most active dipole (with largest current) behaves as a

reflector and the adjacent shorter dipole in front acts as a director. The radiation is then off of the apex. The wedge enclosing the antenna forms an arrow pointing in the direction of the main beam maximum.

As the operating frequency changes, the active region shifts to a different portion of the antenna. The frequency limits of the operational band are roughly determined by the frequencies, at which the longest and shortest dipoles are half-wave resonant, that is,

$$L_1 \approx \frac{\lambda_L}{2} \qquad \text{and} \qquad L_N \approx \frac{\lambda_U}{2} \tag{8.24}$$

where λ_L and λ_U are the wavelengths corresponding to the lower and upper frequency limits. Since the active region is not confined completely to one dipole, often dipoles are added to each end of the array to ensure adequate performance over the band. The number of additional dipoles required is a function of τ and σ. But for noncritical applications, (8.24) is sufficient.

The pattern, gain, and impedance of an LPDA depend on the design parameters τ and σ. Since the LPDA is a very popular broadband antenna of simple construction, low cost, and light weight, we will give the design details and illustrate them by examples. Gain contours are plotted in Figure 8.13 as a function of τ and σ. It should be noted that high gain requires a large value of τ, which means a very slow expansion, that is, a LPDA of large overall length. Gain is only slightly affected by the dipole thickness. It increases about 0.2 dB for a doubling of the thickness. Gain is also affected by the feeder impedance and tends to decrease as the feeder impedance is increased above 100 Ω.

The bottom portion of Figure 8.13 shoes a gain curve that is derived from the data in where *N* the number of dipoles varies from 12 to 47. Notice that the value of $G_{\max}$ is greater than the value of the gain contour at the optimum σ line in the top portion of Figure 8.13. The $G_{\max}$ vs. τ curve probably represents an upper bound on the LPDA gain that can be achieved in practice for feeder impedances of 100 Ω or greater.

Example 8.1: ***Optimum Design of a 54- to 216-MHz Log-periodic Dipole Antenna***

It is desired to have an antenna that operates over the entire VHF-TV and FM broadcast bands, which span the 54- to 216-MHz frequency range for a 4:1 bandwidth. Suppose the design gain is chosen to be 6.5 dB. The corresponding values of τ and σ for a optimum design from Figure 8.13 are

$$\tau = 0.822 \qquad \text{and} \qquad \sigma = 0.149 \tag{8.25}$$

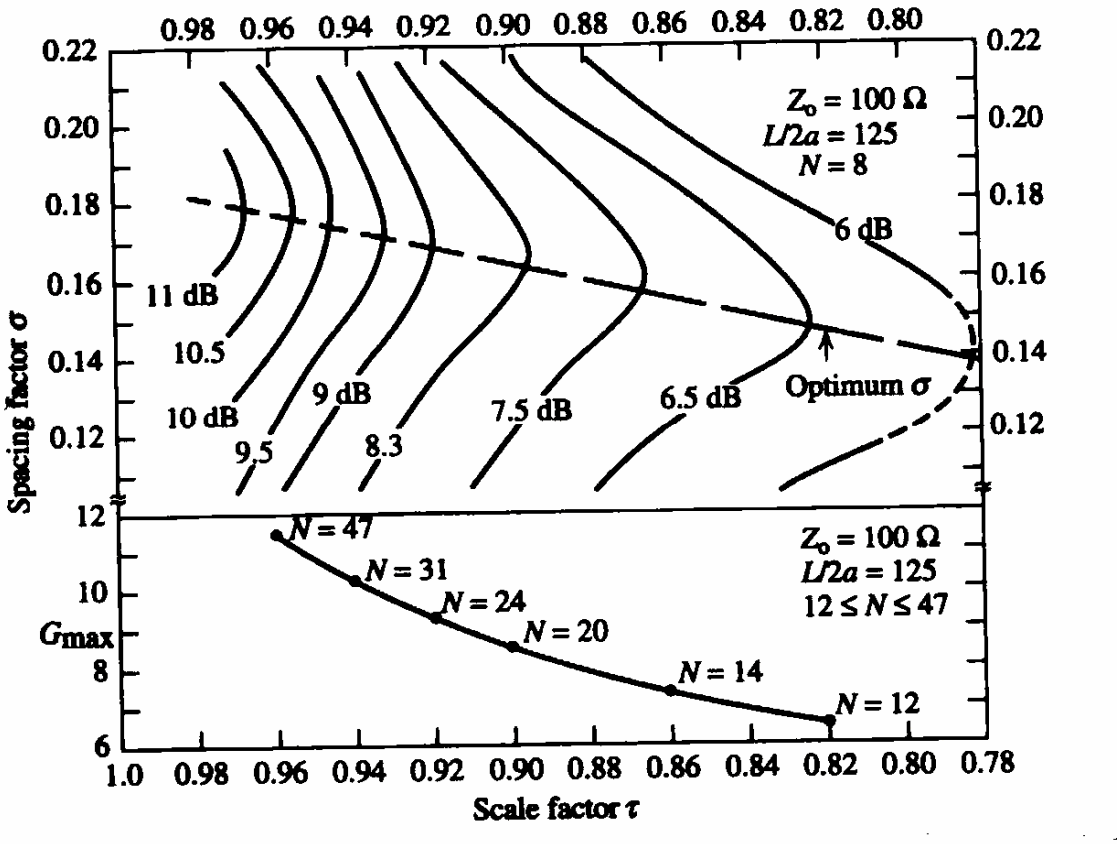

Figure 8.13 Gain of a log-periodic dipole array. {corresponding (top) adapted from Carrel maximum gain curve (bottom) derived from data in }.

Then from (8.2), we have

$$\alpha = 2\tan^{-1}\left(\frac{1-0.822}{4(0.149)}\right) = 33.3^0 \tag{8.26}$$

The length of the longest dipole is determined first. At the lowest frequency of operation (8.54 MHz), the dipole length from (8.24) should be near a half-wavelength, so

$$L_1 = 0.5\lambda_L = 0.5(5.55) = 2.78m \tag{8.27}$$

The shortest dipole length should be on the order of $L_U = 0.5\lambda_U = 0.694m$ at 216 MHz. the LPDA element lengths are computed until a length on the order of 0.694 m is reached. To be specific, element lengths are found from L_1 using $L_{n+1} = \tau L_n$. For example,

$$L_2 = \tau L_1 = (0.822)(2.78) = 2.29 \text{ m}$$

and

$$L_3 = \tau L_2 = (0.822)(2.29) = 1.88 \text{ m}$$

Completing this process leads to

$$\begin{aligned} &L_1 = 2.78 \text{ m}, \quad L_2 = 2.29 \text{ m}, \quad L_3 = 1.88 \text{ m}, \quad L_4 = 1.54 \text{ m}, \\ &L_5 = 1.27 \text{ m}, \quad L_6 = 1.04 \text{ m}, \quad L_7 = 0.858 \text{ m}, \quad L_8 = 0.705 \text{ m} \\ &L_9 = 0.579 \text{ m} \end{aligned} \tag{8.28}$$

The array was terminated with nine elements since $L_9 = 0.579$ m is less than the 0.694 m length for the highest operating frequency. Elements could be added to either end to improve performance at the band edges.

The elements spacing for this example are found from (8.6-83) as

$$d_n = 2\sigma L_n = 2(0.149)L_n = 0.298L_n \tag{8.29}$$

Using the element lengths of d_n are obtained as

$$\begin{aligned} &d_1 = 0.828 \text{ m}, \quad d_2 = 0.682 \text{ m}, \quad d_3 = 0.560 \text{ m}, \quad d_4 = 0.459 \text{ m}, \\ &d_5 = 0.378 \text{ m}, \quad d_6 = 0.310 \text{ m}, \quad d_7 = 0.256 \text{ m}, \quad d_8 = 0.210 \text{ m} \end{aligned} \tag{8.30}$$

The total length of the array is the sum of the spacings in (8.30), which gives a 3.683 m. The outline of the antenna fits into an angular sector of angle $\alpha = 33.3^0$.